Fusion Engineering and Design 130 (2018) 80–88

Contents lists available at ScienceDirect

Fusion Engineering and Design

journal homepage: www.elsevier.com/locate/fusengdes

Effective thermal conductivity of a compacted pebble bed in a stagnant gaseous environment: An analytical approach together with DEM

Akhil Reddy Peeketi[a], Marigrazia Moscardini[b], Akhil Vijayan[a], Yixiang Gan[c], Marc Kamlah[b], Ratna Kumar Annabattula[a,*]

[a] Department of Mechanical Engineering, Indian Institute of Technology Madras, Chennai 600036, India
[b] Institute for Applied Materials (IAM-WBM), Karlsruhe Institute of Technology, 76344 Eggenstein-Leopoldshafen, Germany
[c] School of Civil Engineering, The University of Sydney, NSW 2006, Australia

ARTICLE INFO

Keywords:
Effective thermal conductivity
Pebble bed
Contact conduction
Gap conduction
Discrete Element Method
Granular assembly

ABSTRACT

An analytical estimate of the effective thermal conductivity of a pebble bed with mono-sized pebbles in the presence of a stagnant gas is presented. The Discrete Element Method (DEM) is used to simulate granular assemblies under uniaxial compression and Resistor Network (R-N) model is applied for estimating the effective thermal conductivity numerically. In this paper, two heat transfer paths, i.e., conduction through pebble–pebble contact and pebble–gas–pebble interface are considered. The effect of the cutoff range for gap and the strain on the effective conductivity is studied. The validity of the analytical model is verified with the results from the R-N Model for different solid-to-gas thermal conductivity ratios and for different packing fractions. The analytical and numerical models show a good agreement with the experimental results of the effective thermal conductivity for lithium orthosilicate pebble beds in the presence of helium and air at different temperatures.

1. Introduction

The theoretical prediction of the effective thermal conductivity (k_{eff}) for granular assemblies has been the subject of research for many years. The knowledge of the effective thermal conductivity plays a major role in the design of solid breeder blankets in fusion reactors. These blankets comprise of breeder materials and neutron multipliers in the form of pebble beds in a gaseous environment [1,2]. Similarly, several other energy systems such as pebble bed reactors [3], granular thermal energy storage systems [4] and solid oxide fuel cells [5] require estimation of the effective conductivity of their constituent granular systems.

Batchelor and O'Brien [6] developed a model to estimate the conductance between two adjacent particles in the presence of a fluid. These individual contact conductances were then used to predict the k_{eff} for a granular assembly. With the development of the Discrete Element Method (DEM) [7–12] as a tool to simulate granular assemblies, the accounting for the individual contact conductances at each contact has been made possible. The individual contact conductances were then used to estimate the k_{eff} through different approaches [13–17]. Different conductance relations [18–20] between the adjacent granules were also developed. Several experiments [21–25] have been reported in the literature to establish a parametric correlation for the dependency of the effective conductivity on the microstructural parameters. Even with the development of numerous simulations and experimental data, analytical studies are still helpful. This is because the simulations are computationally expensive and in some cases, it is not feasible to simulate large granular assemblies. Furthermore, analytical solutions may allow to derive an immediate understanding of the relation between parameters. Also, experiments are both time-consuming and expensive. Numerous theoretical models are reported in the literature [26–30] for predicting the effective thermal conductivity of granular assemblies.

Zhao et al. [28] proposed a simple thermal model for the effective thermal conductivity of a monosize and binary pebble beds with stagnant gas in the interstitial spaces. In their model, the pebble bed was assumed to be in a simple cubic lattice configuration. But, the effective conductivity also depends on the granular arrangement, individual interaction between the granules characterized by parameters such as coordination number (N), contact radius (r_c), etc. The model developed by Kovalev and Gusarov [29] includes the effects of these parameters but neglects the effect of conduction due to a fluid in the pore space. In this paper, we attempt to develop a theoretical model that captures the effects of the microstructural parameters of the granular assembly and the presence of fluid in pore space.

In Section 2, an analytical model similar to Kovalev and Gusarov [29], now extended to include the effect of the fluid in the pore space is

* Corresponding author.
E-mail address: ratna@iitm.ac.in (R.K. Annabattula).

https://doi.org/10.1016/j.fusengdes.2018.02.088
Received 29 October 2017; Received in revised form 15 February 2018; Accepted 22 February 2018

proposed for mono-sized granular assemblies. This model includes the heat transfer between adjacent granules which are in contact and also between the granules which are not in contact but separated by a small gap. Only the granular pair (i, j) with a gap width (h_{ij}) less than the cutoff distance (μR) is considered for conduction through the fluid. Here, μ is the cutoff factor and in the further discussion it is referred to as "cutoff". In Section 3, the Resistor Network (R-N) model for calculating k_{eff} is presented. For these models, the conductance relations developed by Batchelor and O'Brien [6] are used as they are in good agreement with experimental results [16]. Due to the low gas velocity, necessary to guarantee tritium extraction in the pebble beds, stagnant condition is considered here. Therefore, the heat transfer due to convection is neglected. The effect of radiation was investigated in [31] and it was found to be negligible for pebble diameters lower than 1 mm from room temperature to 1200 K. Therefore, the contribution due to thermal radiation is also not implemented in this work. The pebbles are assumed to be neither generating nor accumulating any heat. Dalle Donne et al. [21] and Pupeschi et al. [25] studied the influence of gas pressure on the effective thermal conductivity (k_{eff}) of the bed. They found that the k_{eff} depends on the mean free path of the gas molecules and the configuration of the assembly. Such dependence is observed only when the mean free path of the molecules is of the order of interstitial spaces of the pebble bed. For the present model, the influence of gas pressure on the effective thermal conductivity is neglected. The Random Close Packing (RCP) algorithm has been used to generate the granular assemblies and the Discrete Element Method (DEM) is used for simulating uniaxial compression of the pebble assembly which is presented in Section 4. The effect of the cutoff (μ) on k_{eff} is discussed in Section 6 and the evolution of k_{eff} with uniaxial compression is also presented. The proposed analytical model is compared with the experiments performed by Pupeschi et al. [25] for lithium orthosilicate (OSi) pebble beds in the presence of helium and air in Section 6.3. Also, a comparison of the proposed model with other theoretical models reported in the literature [26–29] is presented.

2. Analytical model

In this section, the analytical model for the effective conductivity (k_{eff}) of a 3D mono-sized spherical granular assembly proposed by Kovalev and Gusarov [29] is modified to include the effect of a fluid in the pore space. The microstructural parameters that define the granular assembly are the diameter D (or radius R) of the particles, the packing fraction η, the mean coordination number N, the mean contact radius $\bar{r}_c$ and the angular density of contacts ν. The angular density of the contacts ν is defined as the number of contacts per unit solid angle around a given direction. For an isotropic system, the angular density (ν) is independent of the direction, but for an anisotropic system, ν depends on the direction. In this work, we assume the assemblies to be isotropic as will be justified later.

For a granular assembly, the effective conductivity of the system depends on the conductance between the nearby granules. A schematic of the heat transfer paths between the particles in a granular assembly is shown in Fig. 1a. There are mainly two types of contacts between adjacent granules through which conduction takes place. They are

(a) overlap: through the overlapped area of adjacent granules and the fluid surrounding the overlapped region
(b) gap: through the fluid between adjacent granules.

One can even consider touch contact as a different type as discussed in Batchelor and O'Brien [6]. However, in the derivation of the analytical model, we assume that the contribution of touch type contact is negligible which will be justified in Section 6. Hence, we can consider the conduction between granules to be of two types – gap and overlap. The mean coordination number (N) includes only the overlap type contacts. Hence, one can define a new mean (total) coordination number Z which includes the gap type contacts as well. Let N_o, N_g be the mean coordination numbers of overlap and gap type contacts and p_o, p_g be their relative fractions, respectively such that

$$N_o = N \text{ and } Z = N_o + N_g \tag{2.1}$$

$$p_i = \frac{N_i}{Z} \text{ for } i = o, g \text{ and } p_o + p_g = 1. \tag{2.2}$$

The effective thermal conductivity (k_{eff}) of a granular assembly without any fluid effect is given by Kovalev and Gusarov [29] as

$$k_{\text{eff,nf}} = \frac{\dot{q}}{-\frac{\text{dT}}{\text{dz}}} = \frac{\eta \text{N C}}{\pi D}. \tag{2.3}$$

Here, $\dot{q}$ is the rate of heat flux, dT/dz is the temperature gradient in the direction of heat flow. The conductance C is replaced with effective conductance C^e to include the effect of fluid conductivity in both overlap and gap type contacts. Note that, the overlap contact conductance depends on the fluid and solid where as the gap contact conductance depends only on the fluid. The contact coordination number N should be replaced by the total coordination number Z. The effective conductance C^e can be estimated as

$$C^e = p_o C_o^e + p_g C_g^e \tag{2.4}$$

Here, C_o^e and C_g^e are the effective conductances due to overlap and gap type, respectively for the entire assembly. Hence, the effective conductivity of the granular assembly including the effect of the stagnant fluid is given by

$$k_{\text{eff}} = \frac{\eta Z C^e}{\pi D}. \tag{2.5}$$

Upon substituting C^e from Eq. (2.4),

$$k_{\text{eff}} = \frac{\eta (Z p_o C_o^e + Z p_g C_g^e)}{\pi D} = \frac{\eta (N_o C_o^e + N_g C_g^e)}{\pi D},$$

$$k_{\text{eff}} = \frac{\eta (C_o^t + C_g^t)}{\pi D} = \frac{\eta C^t}{\pi D}. \tag{2.6}$$

where C_o^t and C_g^t are total overlap and gap conductances, respectively and C^t is the total conductance. The gap and overlap contact conductance values are calculated using the relations proposed by Batchelor and O'Brien [6]. A simplified version of these relations for monodisperse assemblies is presented in the following section.

2.1. Conductance relations

Adjacent particles in a granular assembly are considered to possess two types of contacts – overlap and gap. Figs. 2a and b illustrate the particle contact condition. The contact radius $r_{c,ij}$ and the gap width h_{ij} between the particles i and j are defined as

$$r_{\text{c,ij}} = \sqrt{R^2 - \left(\frac{d_{\text{ij}}}{2}\right)^2} \text{ and } h_{\text{ij}} = d_{\text{ij}} - 2R. \tag{2.7}$$

As the particle conductance (C_i^s, C_j^s) and the contact conductance C_{ij}^c are in series as shown in Fig. 2b, the thermal conductance (C_{ij}) between the particles i and j is given by

$$\frac{1}{C_{\text{ij}}} = \frac{1}{C_i^s} + \frac{1}{C_{\text{ij}}^c} + \frac{1}{C_j^s}. \tag{2.8}$$

The contact conductance relations as proposed by Batchelor and O'Brien [6] are adopted in this work with a few modifications. If K_s and K_f are the bulk conductivities of solid and fluid, respectively, then the conductance of each type of contact can be formulated as below,

- Conductance between the overlapped particles i and j with contact radius ($r_{c,ij}$) as adopted by Moscardini et al. [17]

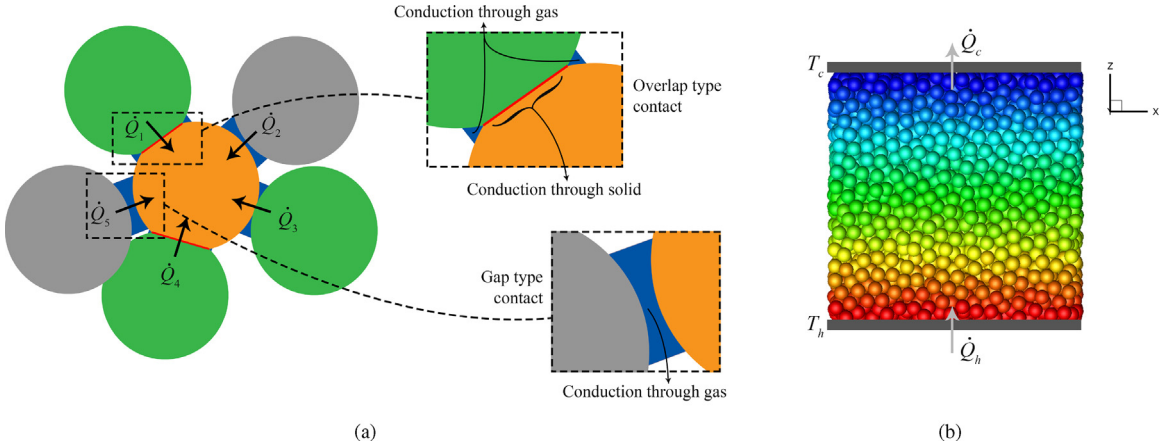

Fig. 1. (a) Schematic of a granular assembly showing the modes of conduction through the solid and gaseous regions for overlap and gap type contacts, (b) Schematic of the temperature distribution in a granular assembly from the DEM simulation with imaginary hot and cold plates at the bottom and top, respectively.

(2.9)$C^c_{o,ij} = \pi K_f R[K_c + \Delta K_g + \ln(\alpha^2)]$where $K_c = 0.22\beta^2_{ij}$ and $\Delta K_g = -0.05\beta^2_{ij}$ for $\beta_{ij} < 1$, linear interpolation for $1 < \beta_{ij} < 100$, $K_c = 2\beta_{ij}/\pi$ and $\Delta K_g = -2\ln(\beta_{ij})$ for $\beta_{ij} > 100$ and $\alpha = K_s/K_f$ and $\beta_{ij} = (\alpha r_{c,ij})/R$.

- Conductance between the neighboring particles i and j with gap width (h_{ij}) by employing a linear interpolation for near touch type region ($0 < \lambda_{ij} < 1$)

$$C^c_{t,ij} = \pi K_f R[(1-\lambda_{ij})\ln(\alpha^2) + \lambda_{ij}\ln(1+\alpha^2\zeta^2)], \quad \text{for } \lambda_{ij} < 1, \tag{2.10a}$$

$$C^c_{g,ij} = \pi K_f R\xi_{ij} \text{ otherwise}, \tag{2.10b}$$

where $\lambda_{ij} = (\alpha^2 h_{ij})/R$, $\xi_{ij} = \ln(1 + \zeta^2 R/h_{ij})$ and ζ is the estimate of the fraction of the mean radius R [14].

Now, for calculating the particle conductance (C^s), the conductance of the half sphere is estimated using its equivalent cylinder. The conductance due to the half particle (C^s) is given by Kanuparthi et al. [14] as

$$C^s_i = C^s_j = C^s = \frac{\pi K_s(\zeta R)^2}{R}. \tag{2.11}$$

The value of ζ is chosen as 0.71 as it was observed to produce good agreement between the numerical and experimental results [17]. The estimation of a newly introduced effective gap (h_e) and its importance in the analytical estimation of effective conductivity (k_{eff}) is discussed in the following subsection.

2.2. Effective gap

It can be observed from Eq. (2.10) that the gap conductance ($C^c_{g,ij}$) is a logarithmic function of the gap width h_{ij}. For calculating the effective gap (h_e), we take the mean of ξ_{ij} ($\bar{\xi}$) over all gap type contacts rather than using the mean of h_{ij} ($\bar{h}$). Therefore, the effective gap (h_e) is estimated as

$$h_e = \frac{\zeta^2 R}{\exp(\bar{\xi}) - 1}. \tag{2.12}$$

It is evident from Fig. 2c that the conductance corresponding to h_e is a better estimate of the mean gap conductance $\overline{C}^c_{g,ij}$ than the conductance corresponding to $\bar{h}$. This is because of the logarithmic dependence of the gap conductance ($C^c_{g,ij}$) on the gap width h_{ij}, thus justifying the use of h_e for the analytical model. The calculation procedure of k_{eff} using the proposed analytical model is presented in the following.

2.3. Calculation of k_{eff} using the analytical model

The values of the microstructural parameters such as mean coordination numbers (N_o, N_g, Z), mean contact radius ($\bar{r}_c$) and effective gap (h_e) are obtained from the DEM simulations. In order to calculate the value of overlap contact conductance (C^c_o) of the entire assembly, we replace $r_{c,ij}$ in Eq. (2.9) with the mean contact radius $\bar{r}_c$ of the assembly. Similarly for the gap contact conductance (C^c_g) of the assembly, h_{ij} in Eq. (2.10) is replaced with the effective gap h_e of the assembly.

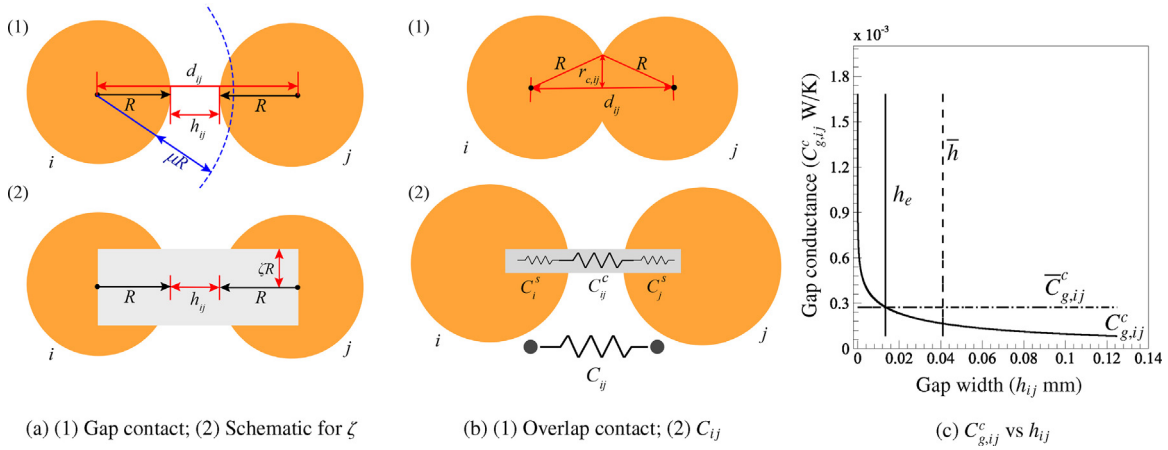

(a) (1) Gap contact; (2) Schematic for ζ (b) (1) Overlap contact; (2) C_{ij} (c) $C^c_{g,ij}$ vs h_{ij}

Fig. 2. (a.1) Schematic showing the condition for gap type contact i.e., $0 < h_{ij} < \mu R$, (a.2) Schematic for the radius of the equivalent cylinder (ζR). (b.1) Schematic for overlap type contact, (b.2) Schematic for the inter-particle conductance (C_{ij}) for the neighboring particles i, j as the particle conductances (C^s_i, C^s_j) and contact conductance (C^c_{ij}) are in series. (c) Gap conductance ($C^c_{g,ij}$) as a function of gap (h_{ij}).

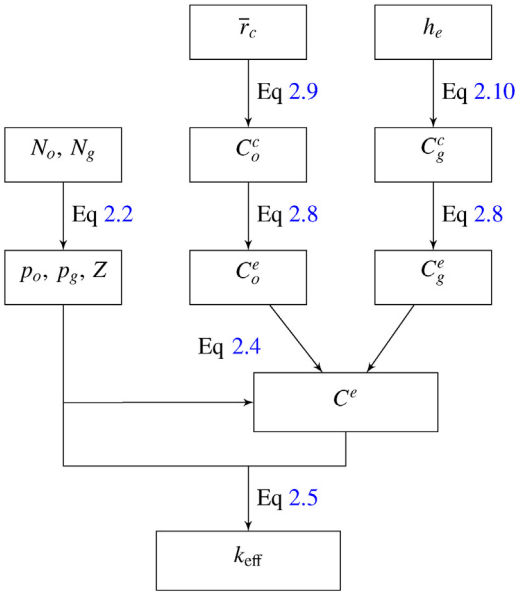

Fig. 3. Flow chart for the calculation of k_{eff} through the analytical model.

The effective overlap and gap conductances (C_o^e, C_g^e) are estimated from the Eq. (2.8) with particle conductance as C^s and contact conductance as C_o^c and C_g^c, respectively. Then, the effective conductance (C_e) can be estimated from Eq. (2.4). Upon estimating the effective conductance (C_e), the k_{eff} can be calculated by Eq. (2.5), where the particle diameter (D) and the packing fraction (η) are known parameters. The steps involved in calculating the k_{eff} through the analytical model from the microstructural parameters are presented in the form of flow chart in Fig. 3.

Resistor Network model is used for validating the proposed analytical model and the results are compared in Section 5. The Resistor Network model for calculating the effective thermal conductivity (k_{eff}) of the pebble bed is presented in the following section.

3. Resistor Network Model

In this section, the Resistor Network (R-N) model for calculating the effective conductivity (k_{eff}) is presented. Consider a periodic granular assembly as described in Section 2. The temperature of the top and bottom layers of the assembly are fixed to simulate imaginary hot and cold plates at bottom and top, respectively as shown in Fig. 1b. The periodic boundary condition is considered for finding the adjacent particles at the sides of the assembly.

Each particle is considered as a node and the resistance between the adjacent particles is taken as a resistor. This creates a network of resistors which in turn can be solved to obtain the total thermal conductance of the system and the temperature of each particle. For solving this network of resistors, a system of linear equations is generated using Ohm's law and Kirchoff's current law as the heat flow rate is analogous to an electric current. At every particle i, the rate of heat flow ($\dot{Q}_{\text{ij}}$) from the particle i to the neighbor particle j is proportional to the temperature difference between them with inter-particle conductance (C_{ij}) being the proportionality constant. Therefore, the heat flow rate from particle i to j is given as

$$\dot{Q}_{\text{ij}} = C_{\text{ij}}(T_i - T_j). \tag{3.1}$$

The conductance (C_{ij}) between the particles i and j is calculated using the relations from [6] presented already in Section 2.1. The sum of the heat flow rates entering and leaving the particle i should be zero as it is neither generating nor accumulating any heat. Hence,

$$\sum_j \dot{Q}_{\text{ij}} + \dot{Q}_i = 0, \tag{3.2}$$

where $\dot{Q}_i$ is the heat flow rate between the particle i and the plate. Hence, $\dot{Q}_i$ will be 0 for every particle i which is not in contact with the plate.

This system of linear equations is then solved using Gauss-Seidel method to obtain the unknown temperatures of the particles and the unknown heat flow rates. The unknown heat flow rate is the heat exchange rate between the particle (contacting the plate) and the plate. The total heat flow rate through the granular assembly can then be estimated as the sum of all the heat flow rates entering/leaving the assembly through the plates. Ideally, the heat flow rate entering the assembly should be equal to the heat flow rate leaving the assembly. However, due to the tolerance used in the Gauss-Seidel method, the solution may not be exact. With the reduction in the tolerance, the system converges to the exact solution at the cost of increase in computational time. In this work, a tolerance of 10^{-4} is used which resulted in a maximum of 2% difference between the heat flow rate entering and the heat flow rate leaving the assembly. Hence, in the following, the mean of the heat flow rate entering and leaving the assembly is used as a measure of the total heat flow rate given by

$$\bar{\dot{Q}} = \frac{\dot{Q}_h + \dot{Q}_c}{2}. \tag{3.3}$$

If A is the cross-sectional area of the granular assembly, ΔT is the temperature difference applied between the plates and Δz is the distance between plates, then the effective conductivity is given by

$$k_{\text{eff}} = \frac{\bar{\dot{Q}}}{A}\frac{\Delta z}{(\Delta T)} = \frac{\bar{\dot{Q}}}{A}\frac{\Delta z}{(T_h - T_c)}, \tag{3.4}$$

where T_h and T_c are the temperatures of the hot and cold plates, respectively. The details of the DEM simulations of random monodisperse assemblies and the validation of the analytical model are presented in the following sections.

4. Simulations

The Random Close Packing (RCP) algorithm has been used to generate granular assemblies. Such a random close packing assembly is then subjected to uniaxial compression using DEM (as developed in [9,10]) where we obtain the new configurations of the assembly with respect to the strain applied. In this paper, lithium orthosilicate (OSi) pebbles in the presence of helium/air are considered as the granular assembly.

The DEM simulations are performed with periodic boundary conditions on all sides to ensure a random packing in the total volume. The assemblies consisted of 5000 OSi pebbles each of 0.5 mm diameter with 4 different initial packing fractions (A: 0.61, B: 0.62, C: 0.63 and D: 0.64). The assemblies from the RCP are then compressed till 1.5% strain along the Z-axis. The Young's modulus, density, Poisson's ratio and the coefficient of friction between the particles are taken as 90 GPa, 2260 kg/m^3, 0.25 and 0.1, respectively. The bed temperature is considered as 25°C. The bulk conductivity of the OSi (K_s) pebbles and the gaseous medium (K_f) as a function of the temperature is given by [32–34]

$$K_s = 7.32 \times 10^{-12}T^4 - 1.30 \times 10^{-8}T^3 + 8.71 \times 10^{-6}T^2 - 0.002876T + 2.620, \quad \text{where } T \text{ is in°C (OSi [32])}, \tag{4.1a}$$

$$K_f = 3.366 \times 10^{-3}T^{0.668}, \quad \text{where } T \text{ is in K (Helium [33])}, \tag{4.1b}$$

$$K_f = -1 \times 10^{-11}T^3 - 4 \times 10^{-8}T^2 + 8 \times 10^{-5}T + 0.0241, \quad \text{where } T \text{ is in°C (Air [34])}. \tag{4.1c}$$

The effective conductivity (k_{eff}) is calculated for the generated assemblies using the R-N model and the analytical model. R-N model

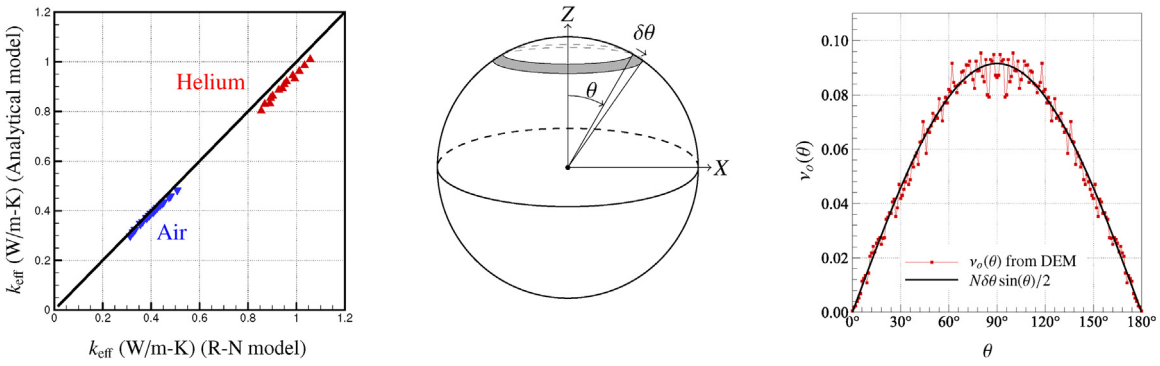

(a) Comparison of analytical and R-N models (b) Calculation of $\nu_o(\theta)$ (c) Distribution of $\nu_o(\theta)$

Fig. 4. (a) Comparison of the effective conductivity (k_{eff}) from the R-N model (X axis) and the analytical model (Y axis) for the assemblies generated by compressing A, B, C and D to different strains in the presence of helium and air, where A, B, C and D correspond to granular assemblies with initial packing fraction of 0.61, 0.62, 0.63 and 0.64, respectively. (b) Schematic showing the hemispherical shaded region defined by ϕ: 0 to 360° and θ for the calculation of angular coordination number $\nu_o(\theta)$. (c) Distribution of angular coordination number $\nu_o(\theta)$ showing the isotropic nature of the random assembly.

requires the configuration (i.e., the coordinates of the particles) of each contact pair in the assembly obtained from DEM as the input. The analytical model requires the specification of the microstructural parameters (N_o, N_g, $\bar{r}_c$, h_e) to estimate the effective thermal conductivity of the bed. These parameters can be obtained directly from the DEM configurations, thereby reducing the complexity of performing numerical thermal simulations to estimate the effective thermal conductivity (k_{eff}) of the pebble bed.

5. Validation of the analytical model

A good agreement between the effective conductivities (k_{eff}) calculated from the analytical model and the R-N model is observed as shown in Fig. 4a. This agreement of results can be attributed to two facts. First is that the analytical model includes the effects of the microstructural parameters and the second, the current assemblies satisfy the assumptions used in the derivation of the analytical model. The analytical model assumes the granular assemblies to be isotropic which is true for the considered assemblies due to the random generation. This isotropic nature can be verified with the help of angular coordination number ($\nu_o(\theta)$) plots. The angular coordination number is defined as the number of contacts per unit polar angle θ (covering the full azimuthal region i.e., ϕ: 0 to 360°). $\nu_o(\theta)$ can be calculated by integrating the angular density (ν) over the hemisphere defined by ϕ: 0 to 360° and θ as shown in Fig. 4b. For isotropic assemblies, the angular density, $\nu(\theta, \phi)$ is given by

$$\nu(\theta, \phi) = \frac{N}{4\pi}, \tag{5.1}$$

$$\nu_o(\theta) = \int_0^{2\pi} \nu(\theta, \phi)\sin\theta \; d\phi\delta\theta \tag{5.2}$$

$$\nu_o(\theta) = \frac{N\delta\theta}{2}\sin\theta \tag{5.3}$$

It can be seen from Fig. 4c that the distribution of ν_o for a sample assembly generated from RCP follows the Eq. (5.3) thus justifying the assumption of isotropic nature. A similar observation was made through tomography experiments by Reimann et al. [35,36]. Further, the temperature distribution along the z direction from the R-N model shows a linear variation (result not shown) justifying the assumption of uniform temperature gradient for the assemblies.

6. Results and discussion

In this section, the effect of cutoff (μ) and strain (ε) on the evolution of the parameters that influence the effective thermal conductivity (k_{eff}) of the granular assemblies is discussed with the help of the proposed analytical model.

6.1. Effect of the cutoff (μ)

The value of the cutoff (μ) determines the extent of gap conduction. As the value of μ increases, new conduction paths are formed increasing the mean gap coordination number (N_g) while the mean overlap coordination number (N_o) remains unaltered. Hence, the relative fraction of the gap coordination (p_g) increases while that of the overlap coordination (p_o) decreases. The variation of mean coordination numbers (Z, N_o, N_g) is shown in Fig. 5a. As the cutoff (μ) increases, the normalized effective gap ($h_{e,n} = h_e/R$) increases as shown in Fig. 5b. This is due to the fact that the increase in μ increases the upper bound of the gap width h_{ij} required for the particles to be in gap type contact. Even though the effective gap (h_e) is a geometrical feature, it is dependent on the fluid because the conductivity of the interstitial fluid determines whether the contact is touch or gap type. For example, consider a gap type contact with normalized gap width (h_{ij}/R) = 1×10^{-5}. For helium as the interstitial gas, this gap contact becomes touch type whereas for air, it will be gap type only (Eq. (2.10)). Since the effective gap conductance (C_g^e) and the effective gap (h_e) are inversely related as shown in Eq. (2.10b), C_g^e reduces with increase in μ. The effective overlap conductance (C_o^e) remains constant with μ as the cutoff (μ) does not affect the mean contact radius ($\bar{r}_c$). As p_o decreases and C_o^e stays constant, the contribution of effective overlap conductance ($p_o C_o^e$) to C^e decreases with μ. Even-though C_g^e decreases, the increase in p_g leads to the increase in the contribution of the effective gap conductance ($p_g C_g^e$) to C^e with μ. The decrease in the contribution of effective overlap conductance is more than the increase in the contribution of effective gap conductance leading to the decrease in effective conductance (C^e) with μ as shown in Fig. 5c.

As μ does not effect the mean overlap coordination number (N_o) and the effective overlap conductance (C_o^e), the total overlap conductance (C_o^t) remains constant with the increase in μ. The total gap conductance (C_g^t) increases with μ as the influence of increase in N_g is greater than that of the decrease in C_g^e. Hence, the total conductance (C^t) increases with increase in cutoff (μ) as shown in Figs. 5d and e, for helium and air, respectively. Note that due to the poor conductivity of air, the increase in total gap conductance due to the increase in μ is less for air compared to the case of helium for the same assembly.

Hence, as the cutoff (μ) increases, the total conductance (C^t) increases leading to the increase in the effective conductivity (k_{eff}) of the assembly as shown in Fig. 5f. In the literature [14,16], it was mentioned that the effective conductivity reaches saturation with the value of cutoff approaching 0.5. Here, this saturation of k_{eff} is observed for the

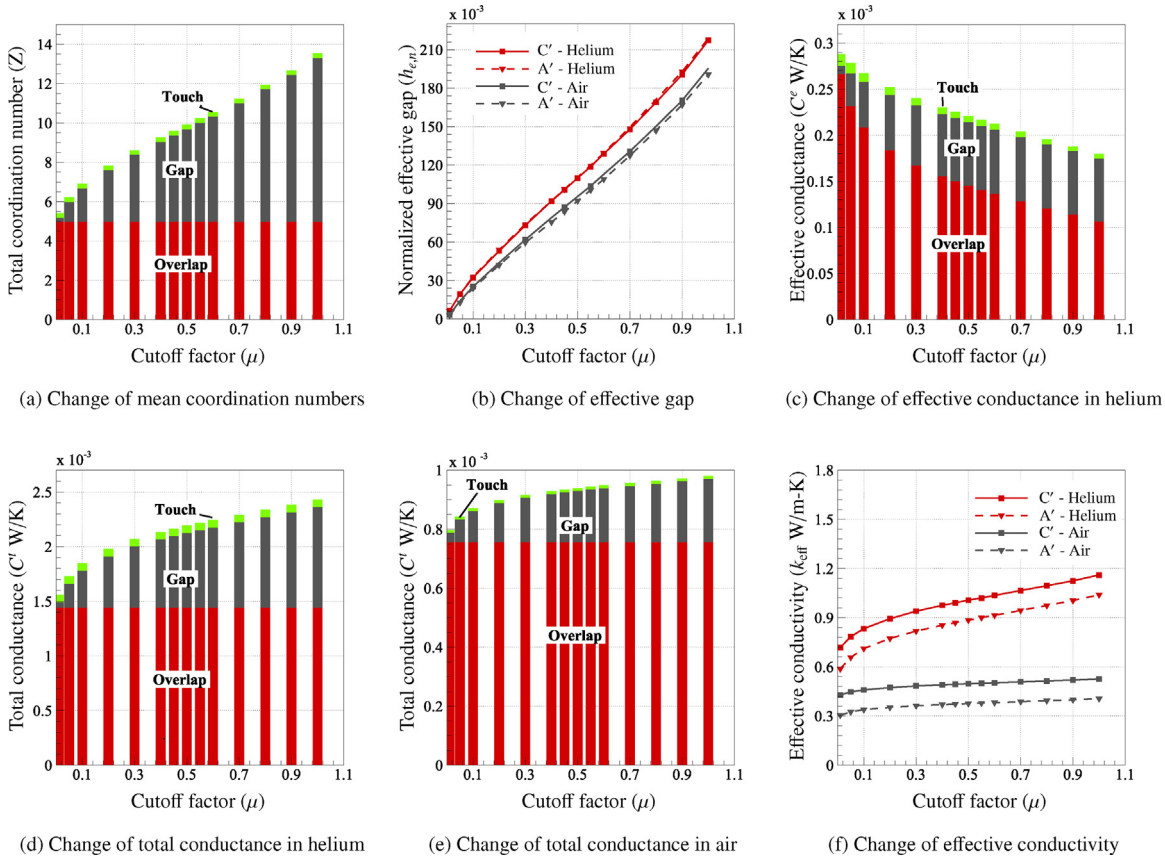

Fig. 5. (a) Effect of cutoff(μ) on the mean coordination numbers (Z, N_o, N_g) for the assembly A′ in the presence of helium. (b) Effect of cutoff (μ) on the effective gap (h_e) for the assemblies A′ and C′ in the presence of helium and air. (c) Effect of cutoff (μ) on the effective conductance (C^e) for the assembly A′ in presence of helium. (d and e) Effect of cutoff (μ) on the total conductance (C^t) for the assembly A′ in the presence of (d) helium and (e) air. (f) Effect of cutoff (μ) on the effective conductivity (k_{eff}) for the assemblies A′ and C′ in the presence of helium and air, where A′ correspond to assembly with initial packing fraction of 0.61 and compressed to 0.75% strain and C′ correspond to assembly with initial packing fraction of 0.63 and compressed to 1.50% strain.

case of air, but for helium, the k_{eff} increases even after $\mu = 0.5$. This can be attributed to the low value of $\alpha(= K_s/K_f)$ for helium ($\alpha = 16.86$) compared to air ($\alpha = 97.83$) at 25°C bed temperature. But, the choice of the value of 0.5 for the cutoff (μ) was observed to fit with experimental results [14,16,17]. Hence, the value of cutoff (μ) is chosen as 0.5 for further studies.

6.2. Effect of the strain (ε)

As the assembly is compressed, new contacts are formed. In addition, the area of contact increases for the already existing overlap type contacts. Further, gap contacts may change to overlap type with increase in strain while the total coordination number (Z) stays almost constant (for moderate strains which induce only a minor displacement of particles). Fig. 6a shows the increase in the mean overlap coordination number (N_o) at the expense of the mean gap coordination number (N_g). Hence, the relative fraction of gap coordination (p_g) decreases while p_o increases with strain (ε). Fig. 6b shows an increase in the normalized effective gap ($h_{e,n}$) with the strain. This may be attributed to the fact that the gap contact pairs having the least gap width (h_{ij}) shift to overlap type under compression. This decreases $\bar{\xi}$ leading to an increase in the effective gap (h_e) because of their inverse relationship (Eq. (2.12)). As p_g decreases and h_e increases with strain, the contribution of the effective gap conductance ($p_g C_g^e$) to the effective conductance (C^e) decreases. Increase in the value of p_o and the mean contact radius ($\bar{r}_c$) leads to an increase in the contribution of the effective overlap conductance ($p_o C_o^e$) to the effective conductance (C^e). The effective conductance (C^e) varies as shown in Fig. 6c with increase in strain for the assembly with an initial packing fraction of 0.61 in the presence of helium. Similar behavior is observed for the assembly in the presence of air as well (results not shown).

As the effective gap conductance (C_g^e) and the mean gap coordination number (N_g) decrease with compression, the total gap conductance (C_g^t) decreases. On the other hand, as the effective overlap conductance (C_o^e) and the mean overlap coordination number (N_o) increase with compression, the total overlap conductance (C_o^t) increases. The resulting variation of total conductance (C^t) with strain (ε) is shown in Figs. 6d and e for helium and air, respectively. In Figs. 6d and e, we can observe that the gap conductance dominates at low strain whereas the overlap conductance dominates at higher strain values. Fig. 6f shows the variation of C_o^t/C_g^t as a function of strain. Note that $C_o^t/C_g^t < 1$ represents the gap dominated region while $C_o^t/C_g^t > 1$ represents the overlap dominated region. It may be noted that a dense granular assembly (case C) approaches the above transition at a lower strain due to the availability of higher number of overlaps compared to a loosely packed assembly. For a given initial packing fraction (i.e., case A or case C in Fig. 6f), the assembly in the presence of air enters the overlap dominating region at a lower strain than the assembly in the presence of helium. The early shift in the case of air may be attributed to its lower conductivity compared to helium.

The increase in effective conductivity (k_{eff}) of the assembly with the increase in strain seems to be marginal as shown in Fig. 7. This may be due to the fact that the total conductance (C^t) is almost constant with increase in compression. Hence, the only factor that contributes to the increase in k_{eff} should be the packing fraction (η) of the assembly as is evident from the analytical model (Eq. (2.6)). Also note that, the percentage increase in the effective conductivity (k_{eff}) is more for the case of air than helium. This is because, the increase in k_{eff} with strain is due

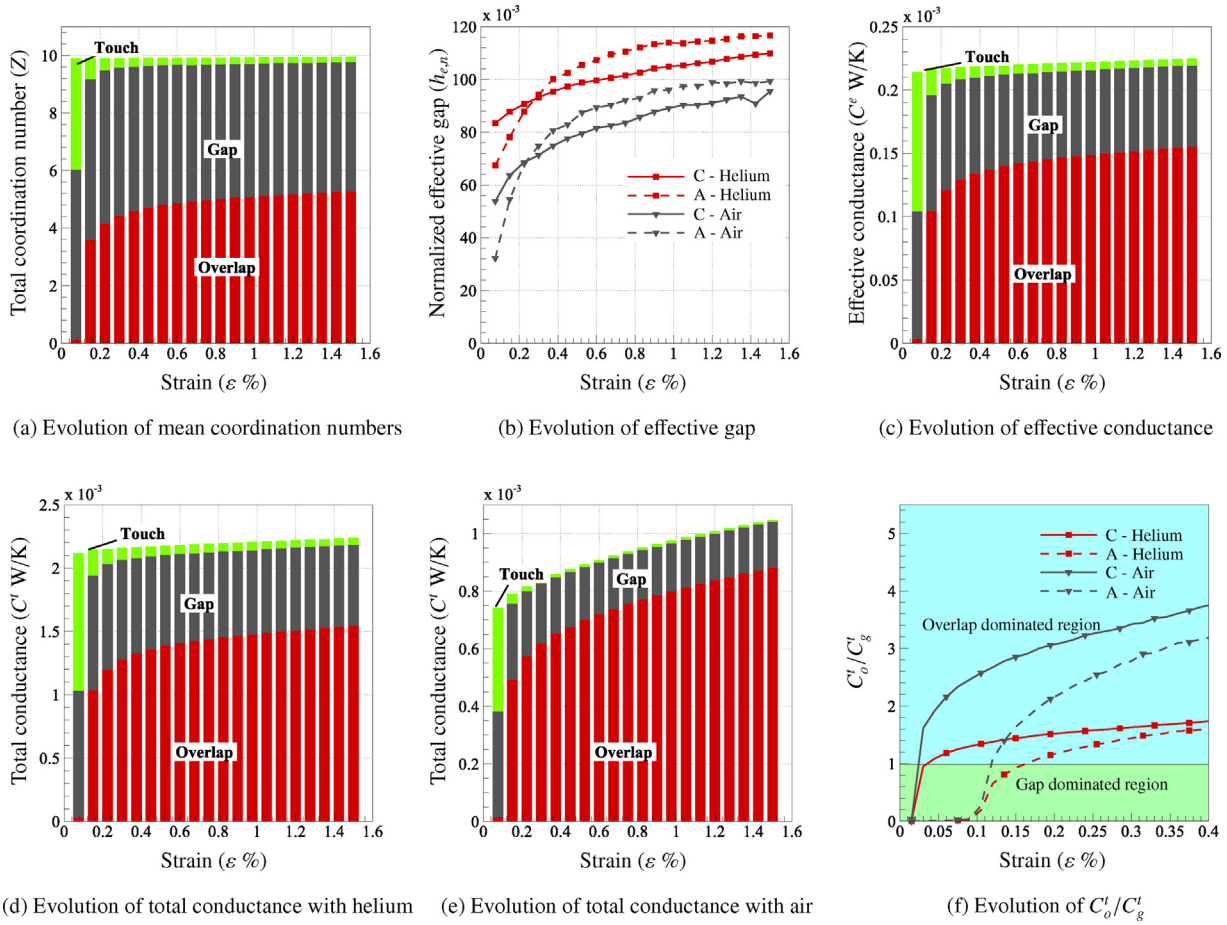

Fig. 6. (a) Effect of strain (ε −%) on the mean coordination numbers (Z, N_o, N_g) for the assembly A in the presence of helium. (b) Effect of strain on the effective gap (h_e) for the assemblies A and C in the presence of helium and air. (c) Effect of strain on the effective conductance (C^e) for the assembly A in the presence of helium. (d and e) Effect of strain on the total conductance (C^t) for the assembly A in the presence of (d) helium and (e) air, respectively. (f) Evolution of C_o^t/C_g^t for assemblies A and C in the presence of helium and air. A and C correspond to the granular assemblies with an initial packing fraction of 0.61 and 0.63, respectively.

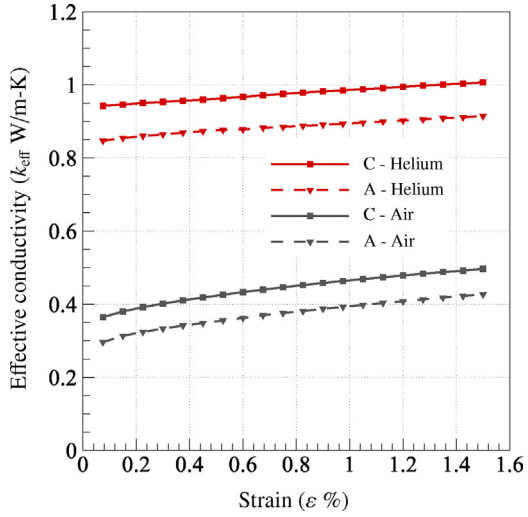

Fig. 7. Evolution of the effective conductivity (k_{eff}) with strain for the assemblies A and C in the presence of helium and air.

to the increase in conduction through the solid phase. Hence, the percentage increase in k_{eff} is less for helium than air as its solid to fluid conductivity ratio (α = 16.86) is low compared to air (α = 97.83). A slight linear increase in the effective conductivity (k_{eff}) with strain was also observed experimentally [22,25]. In this section, it is shown in Figs. 5 and 6 that the contribution of touch type contact is negligible except for very low strains (ε < 0.075%). Thus, the consideration of only gap and overlap type contacts in the analytical model presented in Section 2 is justified.

6.3. Comparison with the experimental results

We use the experimental results of Pupeschi et al. [25] to validate the proposed numerical and analytical models. The experiments correspond to OSi (denoted as EU.Ref in [25]) polydisperse pebble beds with an initial packing fraction of 0.642. The value of the mean diameter ($\overline{D}$ = 0.36 mm) of the polydisperse assembly is taken as the pebble diameter (D) for further analysis. Moscardini et al. [17] have shown the comparison between the simulation and the experimental results reported in the literature, accounting for different pebble materials, different interstitial gases, various bed temperatures and gas pressures. Their numerical simulations reproduce the experimental results with a good agreement by employing ζ = 0.71 and μ = 0.5. Therefore, ζ = 0.71 and μ = 0.5 are used in our work for the validation.

Theoretical models from the literature [26–29] are also plotted for comparison. As seen in Figs. 8a and b, the proposed R-N model and analytical models provide a better estimate than other analytical models. It can be seen that the proposed model fits quite well with experimental results in helium at 4 bar while Hsu et al. [27] fits better with results at 1 bar. The other proposed methods underestimate the effective thermal conductivity in helium. In air, only the presented model is able to predict the experimental results. The good agreement in air and in helium at 4 bar can be explained by the Smoluchowski

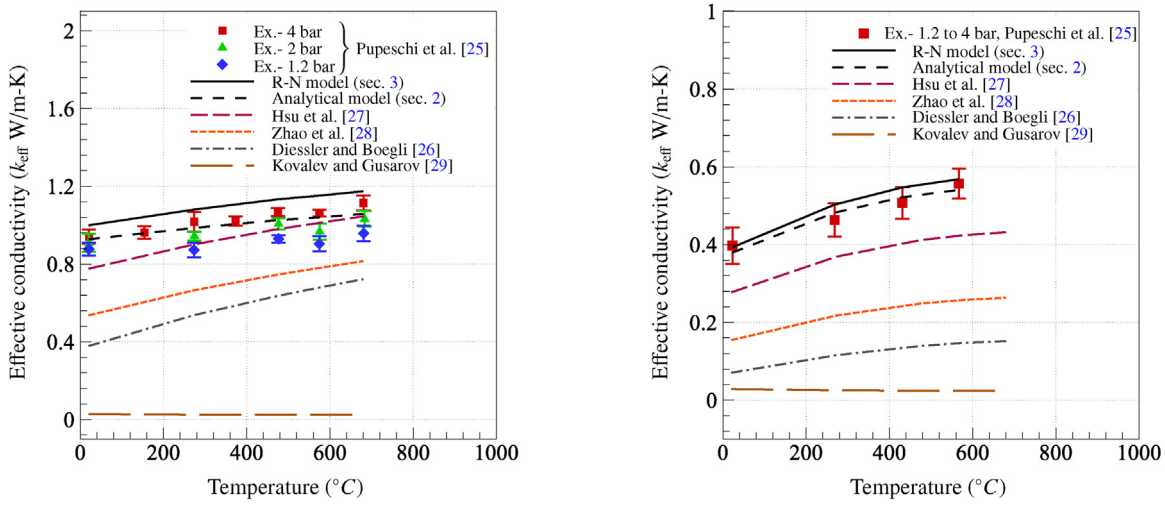

(a) k_{eff} vs T in helium (b) k_{eff} vs T in air

Fig. 8. Comparison of the effective thermal conductivity (k_{eff}) of the OSi pebble bed estimated using the proposed numerical and analytical models with the experiments [25] and also with different theoretical models from literature [26–29] in the presence of (a) helium and (b) air at different temperatures.

effect [37]. The Smoluchowski effect states that the thermal conductivity of a gas decreases with decreasing gas pressure if the gas is confined in small gaps, as in the present scenario. But, the thermal conductivity will be independent of the gas pressure for an unconfined gas. Also, the thermal conductivity of a gas is less in a confined space than in an unconfined space at a given pressure. The mean free path of the interstitial gas molecules increases with the decrease in pressure at a given temperature. As a result, when the mean free path of the gas molecules reaches the order of magnitude of the geometrical dimension of the gas confinement, the thermal conductivity of the gas becomes dependent on its pressure. For the pressures considered in this paper, the Smoluchowski effect is observed predominantly in helium rather than air [25]. Since the mean free path of air is lower than helium, the gas pressure needs to be reduced further for air to show the Smoluchowski effect. Hence, the proposed analytical model may be used for estimating the effective thermal conductivity of a granular assembly in the presence of a gaseous environment with negligible effect of pressure on the gas conductivity.

7. Conclusions

In this paper, an analytical model for estimating the effective thermal conductivity of a pebble bed in the presence of a stagnant gas is proposed. Two types of contacts, i.e., overlap and gap type are considered for the calculation of the effective conductivity. The influence of the cutoff range for gap width and the strain on the evolution of effective thermal conductivity has been presented. The proposed analytical formulation includes the effect of the microstructural parameters such as coordination numbers, contact radius and effective gap resulting in a good agreement with the Resistor Network model.

The gap coordination number (N_g) increases with the cutoff (μ), whereas the overlap coordination number (N_o) is independent of cutoff resulting in a net increase of total coordination number (Z). Even though the total overlap conductance (C_o^t) remains constant, the increase in total gap conductance (C_g^t) leads to the increase in effective conductivity (k_{eff}) with the increase in cutoff (μ). For $\mu > 0.5$, the value of k_{eff} for a pebble bed in the presence of air shows saturation while in the presence of helium k_{eff} continues to increase. The value of μ can be calibrated initially to fit the experimental results.

The overlap coordination number (N_o) increases with increase in strain (ε) at the expense of the gap coordination number (N_g) resulting in an almost constant total coordination number (Z). The total gap conductance (C_g^t) decreases, while the total overlap conductance (C_o^t) increases leading to a slight increase in the total conductance (C^t) with an increase in strain (ε). Hence, the effective thermal conductivity (k_{eff}) shows a slight increase with strain (ε) as observed in the experiments [22,25]. The analytical model matches with the experimental results [25] for air in the pressure range of 1–4 bar as the Smoluchowski effect for air in this regime is negligible. But for helium (in the pressure range of 1–4 bar), the proposed model overestimates the value of k_{eff} as the analytical model does not consider the Smoluchowski effect. Hence, it may be concluded that the proposed analytical model estimates the effective thermal conductivity (k_{eff}) of a pebble bed in a stagnant gaseous environment accurately for the gas pressures where the Smoluchowski effect is negligible.

Acknowledgements

The first author thankfully acknowledges the DAAD-WISE fellowship for allowing him to spend two months as a summer intern at KIT, Germany.

References

[1] J. van der Laan, J. Reimann, A. Fedorov, Ceramic breeder materials, Ref. Module Mater. Sci. Mater. Eng. (2016) 1–63.
[2] A. Ying, J. Reimann, L. Boccaccini, M. Enoeda, M. Kamlah, R. Knitter, Y. Gan, J.G. van der Laan, L. Magielsen, P.D. Maio, G. Dell'Orco, R.K. Annabattula, J.T.V. Lew, H. Tanigawa, S. van Til, Status of ceramic breeder pebble bed thermo-mechanics R&D and impact on breeder material mechanical strength, Fusion Eng. Des. 87 (7) (2012) 1130–1137.
[3] A.C. Kadak, A future for nuclear energy: pebble bed reactors, Int. J. Crit. Infrastruct. 1 (4) (2005) 330–345.
[4] M. Farid, A. Khudhair, S. Razack, S. Al-Hallaj, A review on phase change energy storage: materials and applications, Energy Convers. Manag. 45 (9–10) (2004) 1597–1615.
[5] S. Singhal, Advances in solid oxide fuel cell technology, Solid State Ionics 135 (1) (2000) 305–313.
[6] G. Batchelor, R. O'Brien, Thermal or electrical conduction through a granular material, Proc. R. Soc. Lond. Ser. A Math. Phys. Sci. (1977) 313–333.
[7] P.A. Cundall, O.D. Strack, A discrete numerical model for granular assemblies, Geotechnique 29 (1) (1979) 47–65.
[8] Z. An, A. Ying, M. Abdou, Application of discrete element method to study mechanical behaviors of ceramic breeder pebble beds, Fusion Eng. Des. 82 (15) (2007) 2233–2238.
[9] Y. Gan, M. Kamlah, Discrete element modelling of pebble beds: with application to uniaxial compression tests of ceramic breeder pebble beds, J. Mech. Phys. Solids 58 (2) (2010) 129–144.
[10] R.K. Annabattula, Y. Gan, M. Kamlah, Mechanics of binary and polydisperse spherical pebble assembly, Fusion Eng. Des. 87 (5) (2012) 853–858.
[11] J.T. Van Lew, A. Ying, M. Abdou, A discrete element method study on the evolution

of thermomechanics of a pebble bed experiencing pebble failure, Fusion Eng. Des. 89 (7) (2014) 1151–1157.
[12] H. Zhang, H. Guo, T. Shi, M. Ye, H. Huang, Z. Li, Cyclic loading tests on ceramic breeder pebble bed by discrete element modeling, Fusion Eng. Des. 118 (2017) 40–44.
[13] W. Siu, S.-K. Lee, Transient temperature computation of spheres in three-dimensional random packings, Int. J. Heat Mass Transf. 47 (5) (2004) 887–898.
[14] S. Kanuparthi, G. Subbarayan, T. Siegmund, B. Sammakia, An efficient network model for determining the effective thermal conductivity of particulate thermal interface materials, IEEE Trans. Compon. Packag. Technol. 31 (3) (2008) 611–621.
[15] Y. Feng, K. Han, D. Owen, Discrete thermal element modelling of heat conduction in particle systems: pipe-network model and transient analysis, Powder Technol. 193 (3) (2009) 248–256.
[16] T.S. Yun, T.M. Evans, Three-dimensional random network model for thermal conductivity in particulate materials, Comput. Geotech. 37 (7) (2010) 991–998.
[17] M. Moscardini, Y. Gan, S. Pupeschi, M. Kamlah, Discrete element method for effective thermal conductivity of packed pebbles accounting for the Smoluchowski effect, Fusion Eng. Des. 127 (2018) 192–201.
[18] G. Cheng, A. Yu, P. Zulli, Evaluation of effective thermal conductivity from the structure of a packed bed, Chem. Eng. Sci. 54 (19) (1999) 4199–4209.
[19] Y. Feng, K. Han, C. Li, D. Owen, Discrete thermal element modelling of heat conduction in particle systems: basic formulations, J. Comput. Phys. 227 (10) (2008) 5072–5089.
[20] W. Dai, S. Pupeschi, D. Hanaor, Y. Gan, Influence of gas pressure on the effective thermal conductivity of ceramic breeder pebble beds, Fusion Eng. Des. 118 (2017) 45–51.
[21] M. Dalle Donne, A. Goraieb, G. Piazza, G. Sordon, Measurements of the effective thermal conductivity of a Li_4SiO_4 pebble bed, Fusion Eng. Des. 49 (2000) 513–519.
[22] J. Reimann, S. Hermsmeyer, Thermal conductivity of compressed ceramic breeder pebble beds, Fusion Eng. Des. 61 (2002) 345–351.
[23] H. Tanigawa, Y. Tanaka, M. Enoeda, M. Akiba, Thermal conductivity measurement with silica-coated hot wire for Li_4SiO_4 pebble bed, J. Nucl. Sci. Technol. 46 (6) (2009) 553–556.
[24] D. Mandal, N. Kulkarni, S. Gosavi, C. Mathpati, Experimental investigation of effective thermal conductivity of packed lithium-titanate pebble bed with external heat source and flow of helium, Fusion Eng. Des. 115 (2017) 56–66.
[25] S. Pupeschi, R. Knitter, M. Kamlah, Effective thermal conductivity of advanced ceramic breeder pebble beds, Fusion Eng. Des. 116 (2017) 73–80.
[26] R. Diessler, J. Boegli, An investigation of effective thermal conductivities of powders in various cases, Trans. ASME (1958) 1417–1425.
[27] C. Hsu, P. Cheng, K. Wong, Modified Zehner-Schlunder models for stagnant thermal conductivity of porous media, Int. J. Heat Mass Transf. 37 (17) (1994) 2751–2759.
[28] Z. Zhao, K. Feng, Y. Feng, Theoretical calculation and analysis modeling for the effective thermal conductivity of Li_4SiO_4 pebble bed, Fusion Eng. Des. 85 (10) (2010) 1975–1980.
[29] O. Kovalev, A. Gusarov, Modeling of granular packed beds, their statistical analyses and evaluation of effective thermal conductivity, Int. J. Therm. Sci. 114 (2017) 327–341.
[30] J. Martis, R.K. Annabattula, A semi-analytical model for the effective thermal conductivity of a multi-component polydisperse granular bed, Granul. Matter 19:84 (2017) 1–10.
[31] Y. Asakuma, Y. Kanazawa, T. Yamamoto, Thermal radiation analysis of packed bed by a homogenization method, Int. J. Heat Mass Transf. 73 (2014) 97–102.
[32] B. Löbbecke, R. Knitter, M. Rohde, J. Reimann, Thermal conductivity of sintered lithium orthosilicate compacts, J. Nucl. Mater. 386 (2009) 1068–1070.
[33] Y.Y. Liu, S.W. Tam, Thermal conductivities for sintered and sphere-pac Li_2O and γ-$LiAlO_2$ solid breeders with and without irradiation effects, Fusion Sci. Technol. 7 (3) (1985) 399–410.
[34] The Engineering ToolBox. http://www.engineeringtoolbox.com/dry-air-properties-d_973.html.
[35] J. Reimann, R. Pieritz, C. Ferrero, M. Di Michiel, R. Rolli, X-ray tomography investigations on pebble bed structures, Fusion Eng. Des. 83 (7) (2008) 1326–1330.
[36] J. Reimann, J. Vicente, E. Brun, C. Ferrero, Y. Gan, A. Rack, X-ray tomography investigations of mono-sized sphere packing structures in cylindrical containers, Powder Technol. 318 (2017) 471–483.
[37] G. Springer, Heat transfer in rarefied gases, Adv. Heat Transf. 7 (1971) 163–218.